


Exploring Protein Expression Profiles in Lung Cancer Insufficient Microwave Ablation: Implications for Recurrence

Peng Yan¹, Ruimei Yuan², Zheng Li³, Meili Sun¹ 

¹Department of Oncology, Jinan Central Hospital, Shandong First Medical University, Jinan, People's Republic of China; ²Department of Anesthesiology, Jinan Central Hospital, Shandong First Medical University, Jinan, People's Republic of China; ³Department of Oncology, People's Hospital of Qihe County, Dezhou, People's Republic of China

Correspondence: Meili Sun, Department of Oncology, Jinan Central Hospital, Shandong First Medical University, Jinan, People's Republic of China, Fax +86-0531-55863307, Email smlil980@163.com

Background: Insufficient ablation is a significant factor contributing to the recurrence of non-small cell lung cancer (NSCLC), and it is of great significance to explore the protein expression profile of lung cancer cells after insufficient ablation.

Methods: We establish an insufficient microwave ablation model of lung cancer xenograft in mice, identify differentially expressed proteins (DEPs) and involved signaling pathways through proteomic sequencing, and confirm proteins expression via immunohistochemistry (IHC). Utilizing The Cancer Genome Atlas (TCGA) dataset, we investigate proteins associated with human lung cancer prognosis.

Results: Proteomic sequencing results reveal that 99 proteins exhibited differential expression levels. Subsequent Gene Ontology (GO) and Kyoto Encyclopedia of Genes and Genomes (KEGG) analyses indicate that the DEPs are significantly enriched in metabolic processes. Several DEPs are identified and subsequently confirmed through immunohistochemistry (IHC). Among these proteins, CTP synthase 1 (CTPS1) and Thymidylate synthetase (TYMS), both of which play roles in nucleotide metabolism, are found to be significantly associated with the survival outcomes of patients with lung cancer.

Conclusion: Insufficient ablation can cause alterations in nucleotide metabolism, potentially leading to recurrence and metastasis.

Keywords: lung cancer, thermal ablation, proteomics, nucleotide metabolism

Introduction

Lung cancer stands as the primary cause of cancer-related mortality, responsible for 18.7% of all cancer deaths.¹ The utilization of low-dose spiral CT screening and heightened health consciousness contribute to the detection of a number of early stage lung cancer cases. Pneumonectomy or lobectomy with mediastinal lymph node sampling is considered the standard treatment for early stage non-small cell lung cancer (NSCLC). However, it is estimated that around 20% of patients diagnosed with early stage NSCLC do not undergo surgical interventions due to factors such as poor performance status, advanced age, and comorbidities.² For this type of early lung cancer, stereotactic body radiotherapy (SBRT) or image-guided ablation is recommended.³

Image-guided ablation is a minimally invasive procedure characterized by a brief hospitalization period and absence of radiation-induced damage. For the most popular microwave ablation, demonstrating survival rates are 99% at 1 year, 75.6% at 3 years, and 54.1% at 5 years, whereas cancer-specific survival rates are 99%, 78.9%, and 60.9%, respectively.⁴ Despite outcomes comparable to those of surgical resection and SBRT, challenges such as large tumor size, central location, and irregular morphology are associated with elevated rates of ablation failure.^{5–9} The failure of ablation leads to insufficient tumor destruction, prior research has demonstrated that insufficient ablation resulted in the development of a more aggressive phenotype in residual lung cancer cells, thereby increasing the likelihood of recurrence and metastasis.^{10–12}

Sublethal hyperthermia resulting from insufficient ablation induces a complex regulatory response involving multiple genes and proteins within tumor cells, rather than a singular alteration. While prior research primarily concentrates on individual gene/protein and signaling cascade.^{10–12} In this study, we develop a mice xenograft tumor model of insufficient microwave ablation and employed proteomic analysis to investigate the molecular mechanisms underlying tumor recurrence and metastasis following insufficient ablation.

Methods

Xenograft Tumor Model and Insufficient Ablation

The in vivo mice xenograft model, as described in a previous study,¹³ involved the injection of 2×10^6 Lewis lung carcinoma (LLC) cells into the subcutaneous space on the right flank of C57BL/6 male mice aged 3- to 4-weeks-old and weighing 18~20g. These mice were obtained from Beijing SiPeiFu biotechnology co., LTD. Tumor volumes were assessed using a caliper and calculated using the formula $0.5 \times \text{length} \times \text{width}^2$. The mice were housed under standard laboratory conditions with access to sterilized food and water. Animal welfare practices adhered to institutional and office of laboratory animal welfare guidelines. The LLC cell lines used in this study were obtained from the Science and Innovation Laboratory at Jinan Central Hospital, Shandong First Medical University. The utilization of this cell line and the animal experiments were approved by the Ethical Committee of this institution.

Six mice with subcutaneous tumors were randomly allocated into two groups, each consisting of three mice. The experimental group underwent ablation when the tumor reached a volume of $600 \pm 100 \text{ mm}^3$ using a microwave ablation device (MTC-100, Fuzhong Medical HiTech Co., Ltd. Nanjing, China). Following protocols from previous studies,¹² a lower energy setting was utilized for the ablation procedure, with a power of 5 W and a duration of 30s. To prevent skin scalding, ice was applied to the skin of the mice during the ablation process. A sham-ablation model, involving the insertion of an ablation needle into the tumor without performing ablation, was employed as the control group. In the ablation group, the tumors of the mice were monitored daily. Upon reaching a volume of $600 \pm 100 \text{ mm}^3$ again, the mice were euthanized, and the tumors were removed and preserved in liquid nitrogen. When the tumor volume of the control group reached $600 \pm 100 \text{ mm}^3$, it also was excised and preserved in liquid nitrogen. Ensure that the volume of the two groups was equal when tumors were removed.

Tandem Mass tag (TMT) Proteomics and Data Analysis

The TMT proteomic experimental protocols encompassed sample pretreatment, which involved protein extraction, proteolytic, and TMT labeling, followed by high pH reverse-phase separation, and concluding with data collection and analysis. Specific steps were outlined as follows:

Protein Extraction

Samples were mixed with lysis buffer containing sodium deoxycholate (SDS) and urea, with a protease inhibitor cocktail added. The mixture was homogenized and then centrifuged to determine protein concentration using the BCA method.

Proteolytic

During digestion, 100 µg of protein was reduced with 2 µL of Tris (2-carboxyethyl) phosphine (TCEP) and alkylated with 4 µL of iodoacetamide (IAM). The protein was then precipitated with cold acetone, washed, and re-suspended in triethylammonium bicarbonate (TEAB) buffer. Trypsin from Promega (Madison, WI) was added at a trypsin-to-protein mass ratio of 1:50 and incubated at 37°C overnight. The resulting peptide mixture was desalted using a C18 ZipTip, quantified using the Pierce™ Quantitative Colorimetric Peptide Assay (23275), and subsequently lyophilized using a SpeedVac.

TMT Labeling

Trypsin-digested peptides were labeled with TMT-11Plex reagents (Thermo Fisher Scientific, MA, USA, Art No. A34808) in accordance with the manufacturer's guidelines. Specifically, one unit of TMT reagent was thawed and reconstituted in 50 μ L acetonitrile. Following a 2-hour tagging period at room temperature, hydroxylamine was introduced to react for 15 minutes at room temperature. Subsequently, all samples were combined, desalted, and vacuum-dried.

High pH Reverse-Phase Separation

The peptide mixture was dissolved in buffer A (20 mM ammonium formate in water, pH 10.0) and fractionated using high pH separation on the Ultimate 3000 system with a reverse-phase column. The gradient started at 5% B and increased to 45% B over 40 minutes. B consisted of 20 mM ammonium formate in 80% ACN, pH 10.0. The column was re-equilibrated for 15 minutes at 1 mL/min and 30°C. Six fractions were collected and dried in a vacuum concentrator for processing.

Data Dependent Acquisition

The peptides were dissolved in solvent A (0.1% formic acid in water) and analyzed using an Orbitrap Fusion™ Lumos™ Tribrid™ mass spectrometer connected to an EASY-nanoLC 1200 system (Thermo Fisher Scientific, MA, USA). A 3 μ L peptide sample was injected into a 25 cm analytical column (75 μ m inner diameter, 1.9 μ m resin (Dr Maisch)) and separated using a 60-minute gradient starting at 4% buffer B (80% acetonitrile with 0.1% formic acid) for 1 minute, increasing to 50% over 53.6 minutes, reaching 95% in 40 seconds, and holding at 95% for 5.6 minutes. The column flow rate was 300 nL/min at 55°C, electrospray voltage was 2 kV. Mass spectrometer used DDA mode, switching between MS and MS/MS. Full scan MS spectra (m/z 350–1500) were taken with an Orbitrap at 120,000 resolution. AGC target was 200% with max injection time of 50ms. Precursor ions were fragmented using HCD with 33% collision energy. MS/MS resolution was maintained at 30,000 with a 200% AGC target with the maximum injection time of 54 ms, and dynamic exclusion was 30 seconds.

Data Analysis

The tandem mass spectra were analyzed using PEAKS Studio version 10.6 (Bioinformatics Solutions Inc., Waterloo, Canada) with the Homo sapiens (version 2022, 20610 entries) database obtained from UniProt. Trypsin was selected as the digestion enzyme, and PEAKS DB was searched with a fragment ion mass tolerance of 0.02 Da and a parent ion tolerance of 10 ppm. The maximum number of missed cleavages was set to 2. Carbamidomethylation on cysteine and TMT on lysine and peptide N-terminus were designated as fixed modifications. Oxidation of methionine, acetylation of the protein N-terminus, deamination of asparagine and glutamine were designated as variable modifications. Peptides were filtered at a 1% false discovery rate (FDR) and proteins were filtered based on the presence of at least one unique peptide. Reporter ions were utilized to determine the quantification ratio between samples. Normalization was computed based on the total intensity of all labels in all quantifiable peptides.

Bioinformatics Analysis of Differentially Expressed Proteins (DEPs)

DEPs met the criteria of $|\log_2\text{-fold-change (FC)}| > 1.2$ and $P \text{ value} < 0.05$, were identified utilizing the R package. The volcano plot, a scatter-plot that displayed significance versus fold-change on the y and x axis, respectively, was commonly employed to efficiently detect alterations in large datasets containing replicate data. This plot was generated using the ggplot2 package (<http://ggplot2.org>). Hierarchical cluster analysis, an algorithmic method, is utilized to identify distinct groups with varying levels of similarity or dissimilarity within a dataset, as represented by a similarity matrix. This analysis was processed with pheatmap package ([https://CRAN.R-project.org/](https://CRAN.R-project.org/package=pheatmap) package=pheatmap).

Bioinformatics Analysis of DEPs

The Gene Ontology (GO) annotation and Kyoto Encyclopedia of Genes and Genomes (KEGG) pathway annotation were retrieved from the UniProt database. Fisher's exact test was employed to conduct GO and KEGG enrichment

analyses, respectively. Additionally, a protein–protein interaction network was constructed using STRING v10 (www.string-db.org).

Immunohistochemical (IHC) Analysis

For IHC, tissues embedded in paraffin were sectioned into 5 μm slides. The primary antibodies used in our study were listed below CTP synthase 1 (CTPS1) (Boster #A06374-2, 1:200), Thymidylate synthetase (TYMS) (Boster #BM5360, 1:100), NME nucleoside diphosphate kinase 3 (NME3) (Proteintech #15136-1-AP, 1:200), Renin binding protein (RENBP) (Bioss #bs-8497R, 1:200), Fucose kinase (FCSK) (Sangon #D127113, 1:300), Pyridoxal phosphatase (PDXP) (Abclonal #A17455, 1:300), and Sulfite oxidase (SUOX) (Proteintech #15075-1-AP, 1:200). The staining index was determined by multiplying the staining intensity score by the positive area score. The staining intensity score was as follows: 0, negative; 1, weak; 2, moderate; and 3, strong. The proportion of positive cells was defined as follows: 0 = none; 1 = less than 25%; 2 = 25–75%; 3 = greater than 75%.

Definition of the Gene-Related Prognostic Model in The Cancer Genome Atlas (TCGA) Database

RNA-sequencing expression profiles at level 3 and associated clinical data for lung adenocarcinoma (LAUD) were retrieved from the TCGA dataset. Survival disparities among these groups were assessed using the Log rank test. Univariate and multivariate Cox regression analyses were conducted to determine the appropriate variables for constructing the nomogram. The forestplot R package was utilized to visually represent the *P* value, hazard ratio (HR), and 95% confidence interval (CI) for each variable.

Multivariate Cox regression analysis was employed to develop a multi-gene prognostic model, utilizing the R package survival for the analysis. Kaplan–Meier curves, *P* value, and HR with 95% CI were derived through Log rank tests and univariate Cox proportional hazards regression. All analytical techniques and R packages were executed using R (Foundation for Statistical Computing, 2020) version 4.0.3, with a significance level set at $P < 0.05$.

In accordance with the Article 32, Item 2, of the Measures for Ethical Review of Life Science and Medical Research Involving Human Subjects, enacted on February 18, 2023, in China, research utilizing legally obtained publicly available data or observational data that does not interfere with public behavior is eligible for exemption from ethical review. Consequently, this study was granted such an exemption, which was formally approved by the Research Ethics Committee of Jinan Central Hospital, Shandong First Medical University.

Statistical Analysis

Unpaired Student's *t* test was used to compare two groups, with distributed variables and values are expressed as the mean \pm SD. All statistical analyses were performed using GraphPad Prism 8.0. Significance was determined at $P < 0.05$.

Results

Differentially Expressed Proteins in Insufficient Ablation and Sham-Ablation Tumors

Differential expression analysis showed that 99 proteins were differentially expressed between the ablation group and the control group, with 94 proteins up-regulated and 5 proteins down-regulated ([shown in supplementary materials 1](#)). These results were visualized by a volcano plot, shown in [Figure 1A](#). The DEPs expression levels of regulated proteins were illustrated by the hierarchical clustering heatmap in [Figure 1B](#), where red represents up-regulated proteins and green represents down-regulated proteins.

Functional Characterization of DEPs

GO and KEGG enrichment analyses of all 99 DEPs were performed to explore their biological functions ([Figure 2](#)). Biological process from GO enrichment at different levels were shown in [Figure 2A](#). At level 1, a total of 59 DEPs were identified to be associated with metabolic processes. Moving to level 2, the predominant biological processes were nitrogen compound metabolic processes, cellular metabolic processes, primary metabolic processes, and

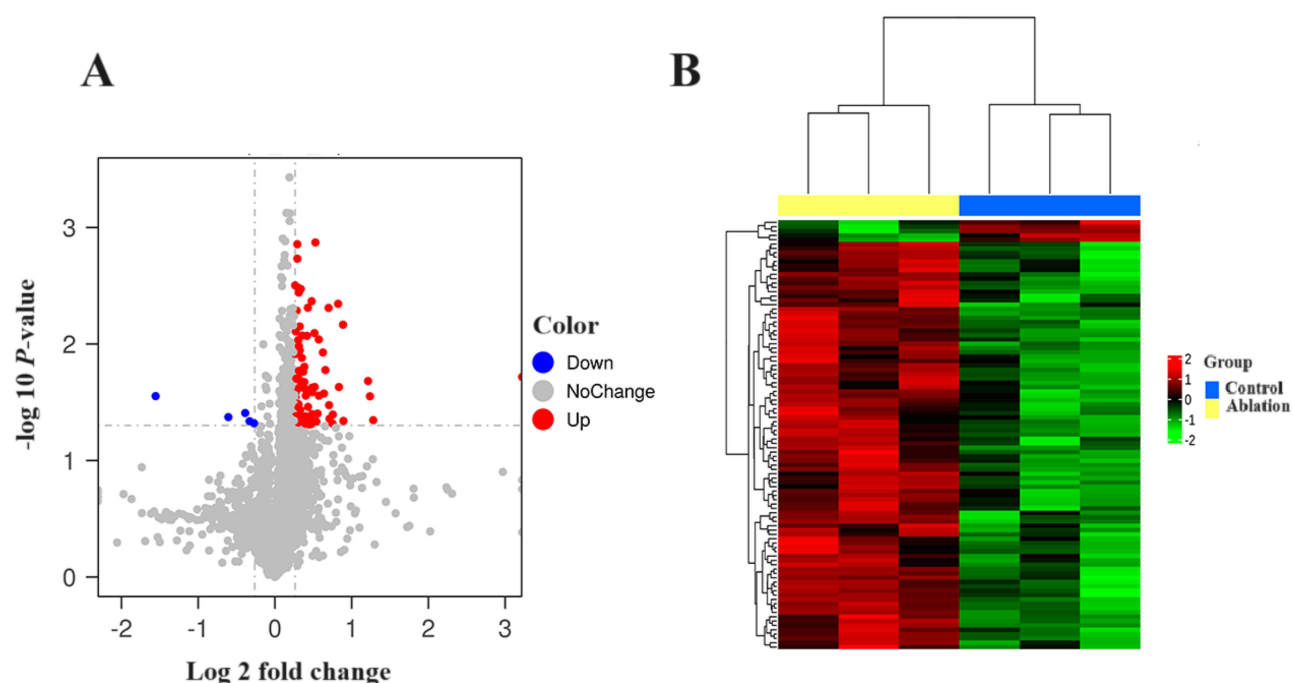


Figure 1 Identification of DEPs in insufficient ablation and sham-ablation tumors. **(A)** Volcano plot showing DEPs in insufficient ablation group and untreated group within xenograft tumor model. **(B)** The hierarchical clustering heatmap of DEPs in insufficient ablation group and control group within xenograft tumor model.

organic substance metabolic processes. Progressing to level 3, the most notable enrichment was observed in the organonitrogen compound metabolic process and the macromolecule metabolic process. At level 4, the prominent biological processes included macromolecule modification, protein metabolic processes, and cellular macromolecule metabolic processes.

The results of KEGG enrichment analysis depicted in Figure 2B illustrated the prominent biological pathways identified. The analysis revealed significant enrichment in two major pathways related to metabolism and genetic information processing. Metabolism processing included nucleotide metabolism, biosynthesis of cofactors, amino sugar and nucleotide sugar metabolism, sulfur metabolism, pyrimidine metabolism, vitamin B6 metabolism. While genetic information processing included basal transcription factors, ribosomes, and protein processing in the endoplasmic reticulum.

Protein-Protein Interaction (PPI) Network Analysis of DEPs

The analysis revealed that 26 proteins within the DEPs were found to interact with other proteins (shown in [supplementary materials 2](#)). Notably, proteins with degree values exceeding 9 included Ubiquilin 1 (UBQLN1), ATR serine/threonine kinase (ATR), CTPS1, AlkB homolog 8 (ALKBH8), Mitochondrial ribosomal protein S7 (MRPS7), TYMS, Mitochondrial ribosomal protein L17 (MRPL17), Eukaryotic translation initiation factor 2 alpha kinase 4 (EIF2AK4), M-phase phosphoprotein 8 (MPHOSPH8), Bromodomain containing 8 (BRD8), Component of inhibitor of nuclear factor kappa B kinase complex (CHUK), Cell division cycle 23 (CDC23), and NME3 (as shown in Figure 3).

Core Proteins Were Identified Through Bioinformatics Analysis

Shown as in Figure 4, the Sankey diagram was utilized to identify the core proteins in GO and KEGG enrichment. The results illustrated that CTPS1, TYMS, NME3, PDXP, RENBP, FCSK, and SUOX were selected for additional validation analysis. The variations in abundance levels and statistical significance of the DEPs were presented in Table 1 detected by proteomic sequencing.

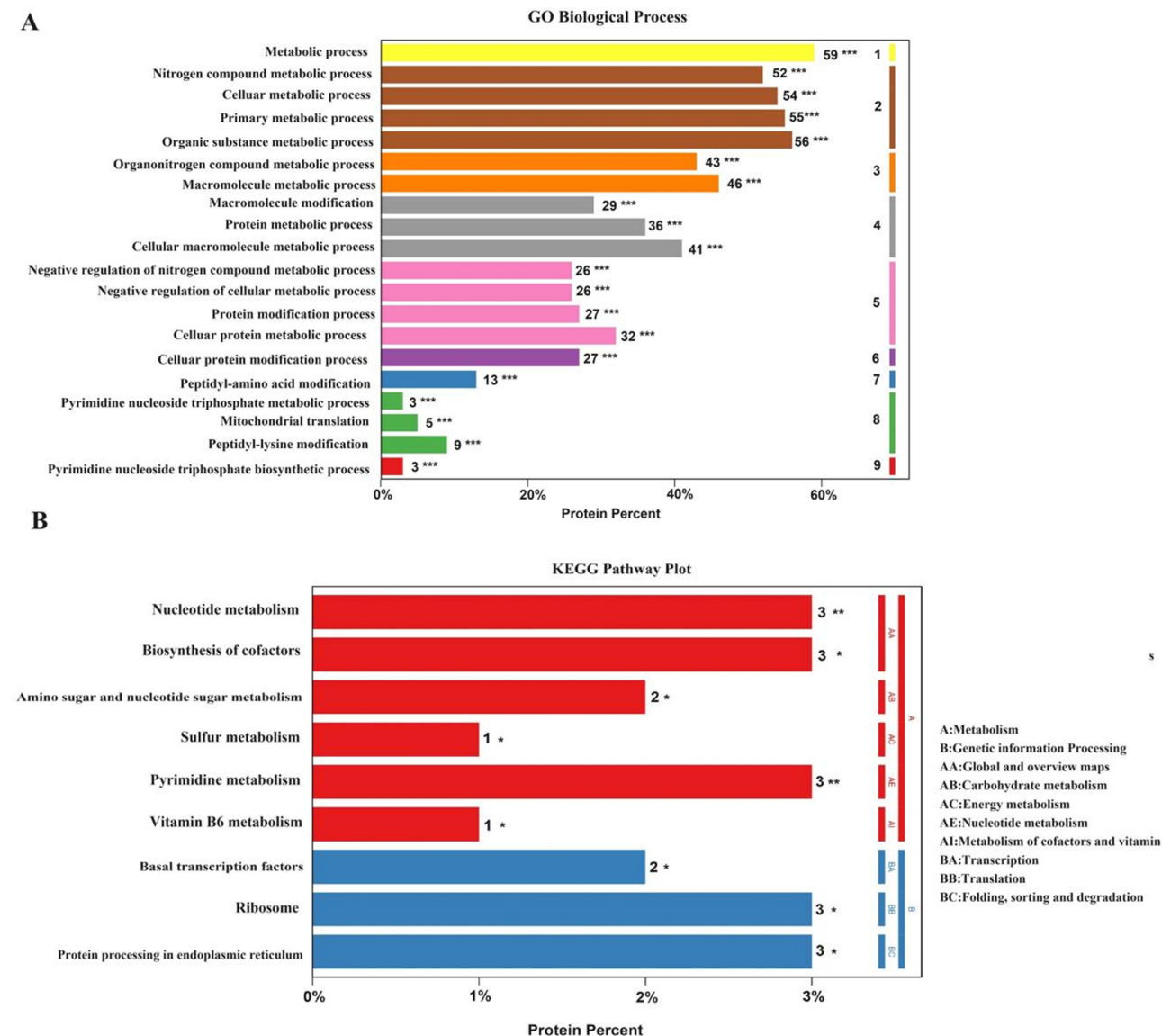


Figure 2 Bioinformatics analysis of differentially expressed proteins. **(A)** Biological processes of GO analysis were organized by p-values, with the horizontal axis representing the percentage of enriched proteins in each term. The number following each term indicated the quantity of distinct proteins involved. The left axis corresponded to the biological process term, while the right axis corresponded to the GO level. **(B)** The KEGG analysis displayed the enriched metabolic pathways, with the left ordinate indicating the pathway enriched and the right ordinate showing the abbreviations of the primary and secondary classification names of the enriched pathways in a hierarchical manner. * $P < 0.05$; ** $P < 0.01$; *** $P < 0.001$.

Validation by Immunohistochemistry

IHC was employed to confirm the expression of the identified proteins in the model of insufficient ablation of xenograft tumors. As shown in Figure 5A and B, the findings indicated a significant upregulation of CTPS1, TYMS, and RENBP in the insufficient ablation tumors, whereas SUOX expression was decreased. No statistically significant differences were observed in the expression levels of NME3, PDXP, and FCSK.

The Correlation Between DEPs and Prognosis in Lung Adenocarcinoma

Data from The Cancer Genome Atlas (TCGA)-LAUD database was utilized to investigate the potential association between the differentially expressed genes mentioned above and the prognosis of human lung cancer. The Cox regression analysis was performed to evaluate the prognostic from various clinicopathological variables including age, gender, TNM stage, and smoking status. The results are shown in Table 2. The study findings indicated

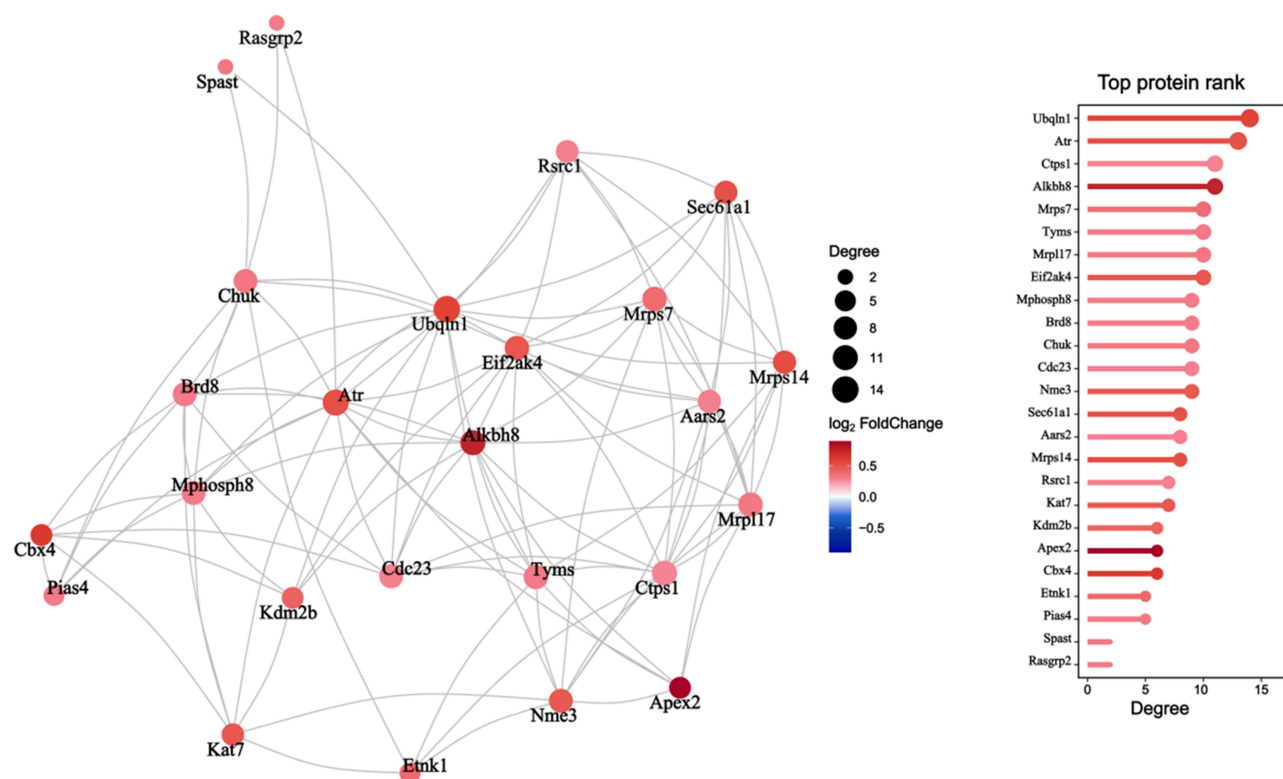


Figure 3 PPI network of DEPs constructed using STRING. The protein-protein interaction network of DEPs was constructed using the STRING database. In the interaction network diagram depicting the top connectivity proteins, circles symbolize the DEPs, with red indicating up-regulation and blue indicating down-regulation. The size of the circle corresponds to the level of connectivity, with larger circles representing higher connectivity. The accompanying graph illustrated the expression histogram of the top connectivity proteins.

a significant association between CTPS1 and TYMS expression levels and overall survival (OS) in patients. The Kaplan–Meier survival curve was evaluated in two groups stratified by the median risk score. The results revealed that lung adenocarcinoma patients with high CTPS1 expression had a median survival time of 3.5 months, compared to 4.4 months for those with low expression (HR = 1.34, $P = 0.0465$) (Figure 6A). Similarly, patients with high TYMS expression had a mOS of 3.5 months, in contrast to those with low expression had a mOS of 4.5 months, HR = 1.63, $P = 0.00115$ (Figure 6B).

A multiple-gene risk model was explored (Figure 6C). The Kaplan–Meier survival curve was applied to present a comparison of the OS of the two groups divided by the median risk score. Besides, the area under the receiver operator characteristic curve (ROC) curve (AUC) of the time-dependent ROC curve was used to assess the prognostic ability of the double-genes signature, and a higher AUC meant the better the model performance. We found that there was a significant difference in OS between the high- and low-risk groups (3.4 months vs 4.5 months, $P = 0.000566$). The AUCs of the double-gene signature corresponding to 1, 3, and 5 years of survival were 0.611, 0.615 and 0.602, respectively, suggesting that the prediction model had high sensitivity and specificity.

Discussion

Several studies have investigated the underlying mechanisms through which insufficient ablation contributed to the recurrence of lung cancer. Peng B et al research demonstrated that heat shock protein 70 (HSP70) inhibited ferroptosis by facilitating HIF-1 α SUMOylation, thereby promoting lung cancer recurrence following insufficient ablation.¹⁰ Additionally, Wang J et al study revealed that insufficient ablation enhanced the proliferation of NSCLC cells through the activation of PI3K/Akt/HIF-1 α signaling pathways.¹¹ Furthermore, our previous research indicated

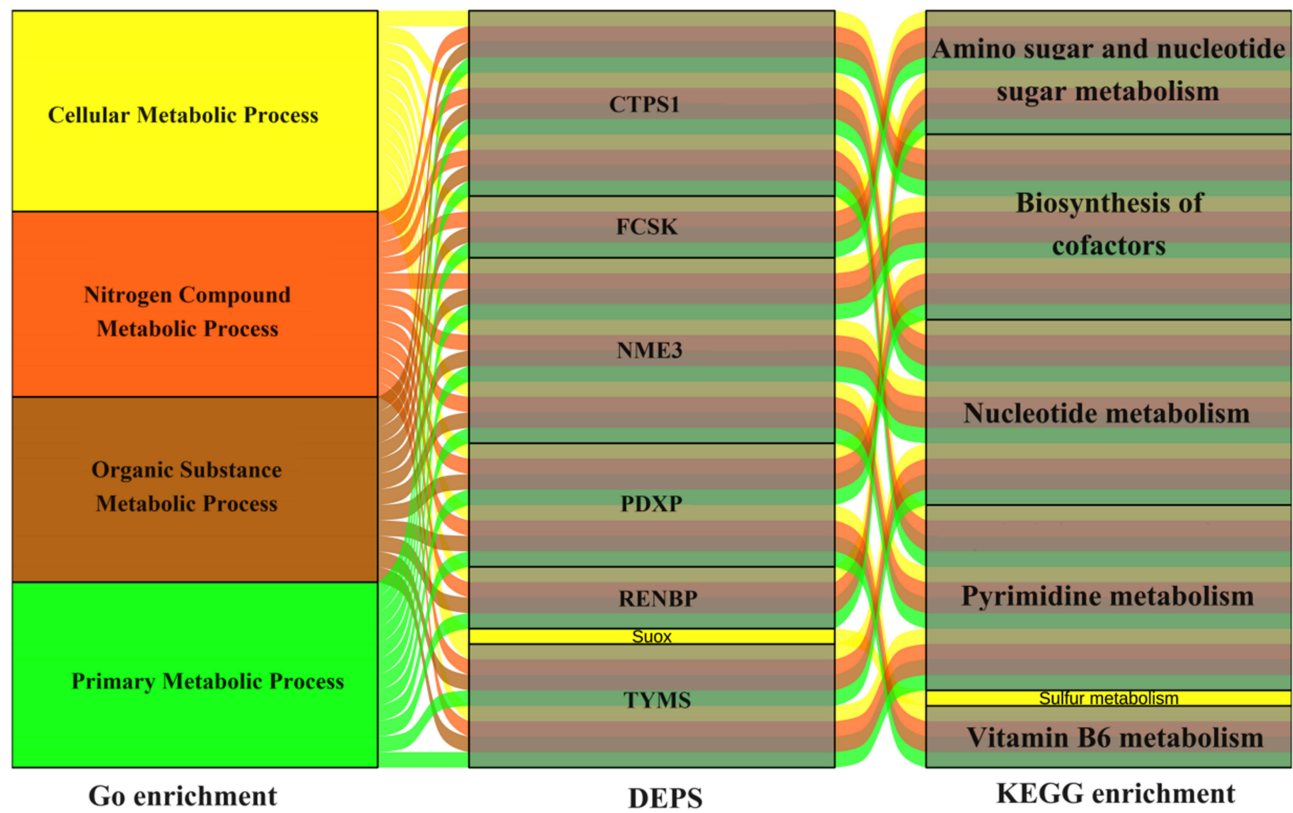


Figure 4 The Sankey diagram illustrated the relationship between the TOP KEGG pathways and the TOP GO biological processes of the most significant proteins. The left column represented the GO biological processes, the middle column displayed the DEPs, and the right column indicated the KEGG enrichment pathways.

that insufficient ablation may induce epithelial mesenchymal transition (EMT) in residual tumor cells by upregulating Carboxypeptidase A4.¹² The effects of thermal stimulation on genes and proteins expression were intricate, involving the activation or inhibition of multiple signaling pathways that work in conjunction with one another. However, previous studies have predominantly focused on individual gene/protein and signaling pathway. Consequently, this study utilized proteomics to investigate the significant alterations in pathways and proteins following thermal stimulation in NSCLC resulting from insufficient ablation for the first time.

Based on an analysis of differential protein expression profiles, GO analysis, and KEGG analysis, it was postulated that tumor progression may activate multiple metabolism-related signaling pathways, resulting in metabolic reprogramming. The identified key differential proteins, including CTPS1, TYMS, RENBP, and

Table I Differential Expression Proteins

Gene Names	Protein Names	Fold Change	P value
TYMS	Thymidylate synthase	1.24	0.017
CTPS1	CTP synthase I	1.22	0.036
NME3	Nucleoside diphosphate kinase 3	1.39	0.004
RENPB	Renin binding protein	1.23	0.041
FCSK	Fucokinase	1.24	0.010
PDXP	Pyridoxal phosphatase	1.28	0.008
SUOX	Sulfite oxidase	-1.52	0.042

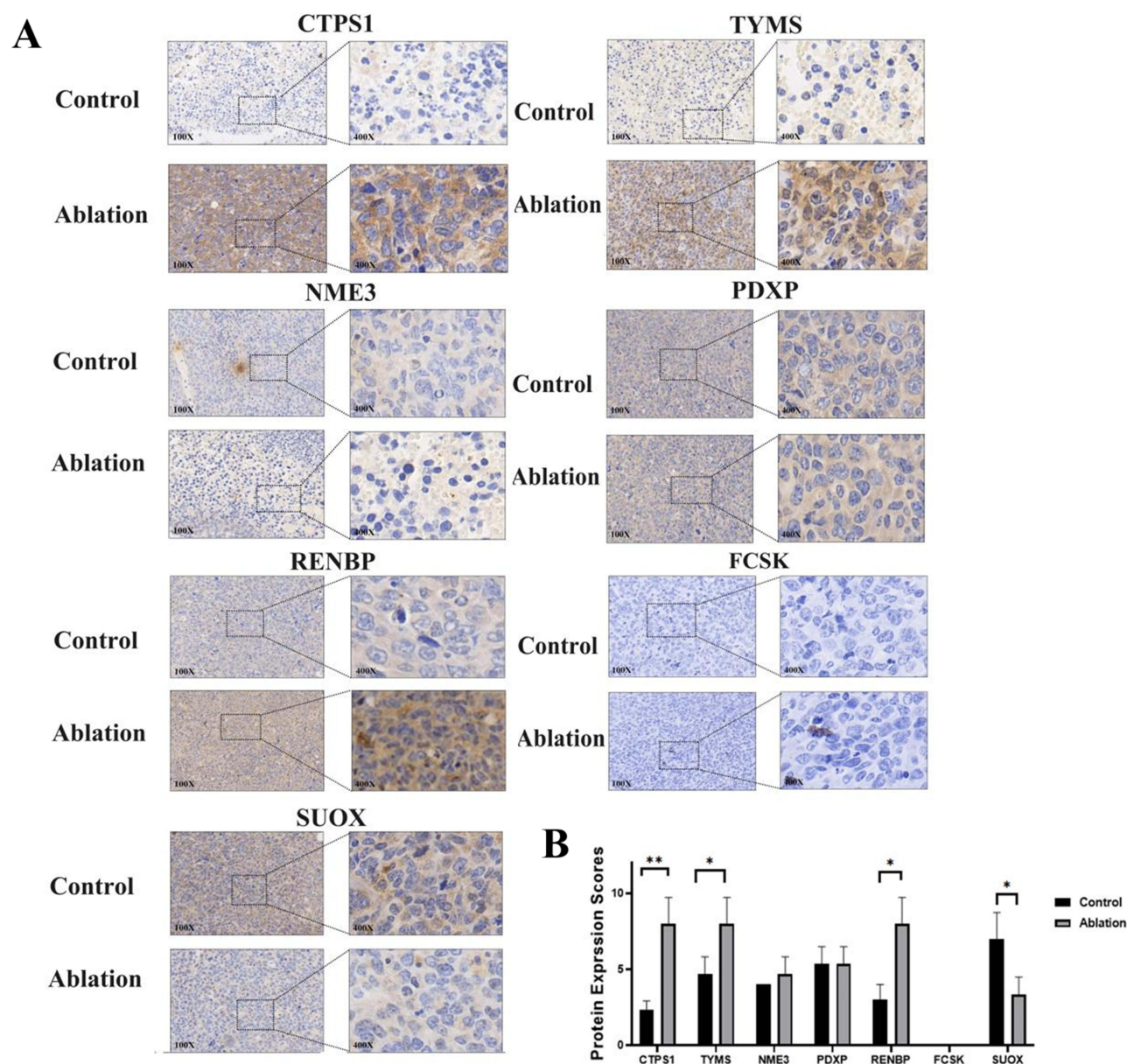


Figure 5 Immunohistochemical analysis in insufficient ablation and sham-ablation tumors within xenograft tumor model. **(A)** Immunohistochemical representative images in insufficient ablation and the control groups. The left column was magnified by 100, while the right column was magnified by 400 in the images. **(B)** Statistical analysis of varying protein expression levels in the two groups. * $P < 0.05$, ** $P < 0.01$.

SUOX were further investigated through immunohistochemistry to confirm differential expression in tumors following insufficient ablation.

In order to investigate the potential correlation between a subset of the aforementioned DEPs and the prognosis of human tumors, the TCGA dataset was employed. Our analysis, which included the Kaplan–Meier survival curve as well as univariate and multivariate Cox regression analyses, confirmed a significant association between CTPS1 and TYMS expression levels and prognosis. These two genes with significant prognostic implications were identified and utilized to develop a prognostic multiple gene signature survival prediction. The CTP nucleotide played a crucial role as a precursor in nucleic acid metabolism, particularly in the process of DNA replication. The de novo synthesis of CTP is dependent on the enzymatic activity of CTP synthetases 1 and

Table 2 Relationship Between DEPs and Prognosis From TCGA Dataset

	Univariate COX Regression		Multivariate COX Regression	
Gene Names	HR (95% CI)	P value	HR (95% CI)	P value
CTPS1	1.28(1.06,1.54)	0.010	1.20(1.00,1.45)	0.055
TYMS	1.34(1.15,1.57)	0.0003	1.27(1.07,1.50)	0.006
NME3	0.99(0.83,1.19)	0.915	1.02(0.84,1.23)	0.853
RENBP	0.86(0.74,0.99)	0.035	0.92(0.79,1.07)	0.270
FCSK	0.86(0.69,1.07)	0.165	0.86(0.68,1.09)	0.204
PDXP	1.29(0.49,3.40)	0.601	1.21(0.46,3.17)	0.705
SUOX	0.79(0.62,1.00)	0.058	0.74(0.58,0.99)	0.022

2 (CTPS1 and CTPS2), which facilitate the conversion of UTP to CTP. Notably, CTP synthetase activity was elevated in rapidly dividing cells, such as cancer cells.^{14,15} It has been observed that CTPS1 exhibited greater efficacy in promoting cell proliferation compared to CTPS2, likely due to its higher intrinsic enzymatic activity and increased resistance to inhibition by 3-deaza-uridine, a UTP analog.¹⁶ TYMS was a crucial enzyme that relies on folate for its function, producing the sole intracellular source of deoxythymidine monophosphate (dTMP) necessary for DNA synthesis and repair. Moreover, increased expression of TYMS mRNA and protein has been linked to a poor prognosis in various solid tumor.^{17–19} Both of these genes played essential roles in the nucleotide metabolism pathway. We hypothesize that insufficient ablation may trigger activation of the nucleotide metabolism in residual tumor cells, subsequently inducing metabolic reprogramming.

Metabolic dysregulation was a prominent characteristic of cancer cells, with the increased production and utilization of nucleotide triphosphates serving as a crucial and consistent metabolic requirement across various cancer types and genetic profiles. The aggressive phenotypes exhibited by cancer cells, such as uncontrolled proliferation, resistance to chemotherapy, evasion of immune surveillance, and metastasis, heavily rely on enhanced nucleotide metabolism. Moreover, the majority of identified oncogenic drivers stimulated the augmentation of nucleotide biosynthesis, indicating that this metabolic trait was essential for the initiation and progression of cancer.²⁰ Insufficient ablation-induced sublethal heat damage led to activation of the nucleotide metabolic pathway, resulting in the development of aggressive phenotypes in residual tumor cells.

Our research findings held some degree of importance. First, the hypothesis that insufficient ablation may intervene nucleotide metabolism and subsequently induce metabolic reprogramming has been posited and substantiated. Furthermore, agents targeting nucleotide metabolism, such as 5-Fluorouracil,²¹ pemetrexed,²² and gemcitabine,²³ which target thymidylate synthase and ribonucleotide reductase, respectively, could potentially serve as a strategy for adjuvant or salvage treatment resulting from NSCLC ablation recurrence.

Nevertheless, our study has some limitations. First, the sample size is extremely small. Second, the research is conducted using a mouse model, and it remains unknown whether insufficient ablation could elicit similar biological changes in human lung cancer. Human lung tumor tissues post-recurrence for IHC would provide more compelling evidence. However, the local control rate of early stage lung cancer following ablation has been reported to be between 73% and 96% at one year and between 65% and 80% at three years, indicating a recurrence rate of only 20% to 35% at three years.^{24,25} While selecting histological samples from recurrent biopsies at a three-year follow-up would be more informative, it necessitates a substantial number of samples and an extended follow-up period. Additionally, further investigation into blocking nucleotide metabolism pathway after insufficient ablation should also be observed in future.

In conclusion, this study reveals that insufficient microwave ablation results in the reprogramming of nucleotide metabolism, potentially contributing to the recurrence and metastasis following ablation.

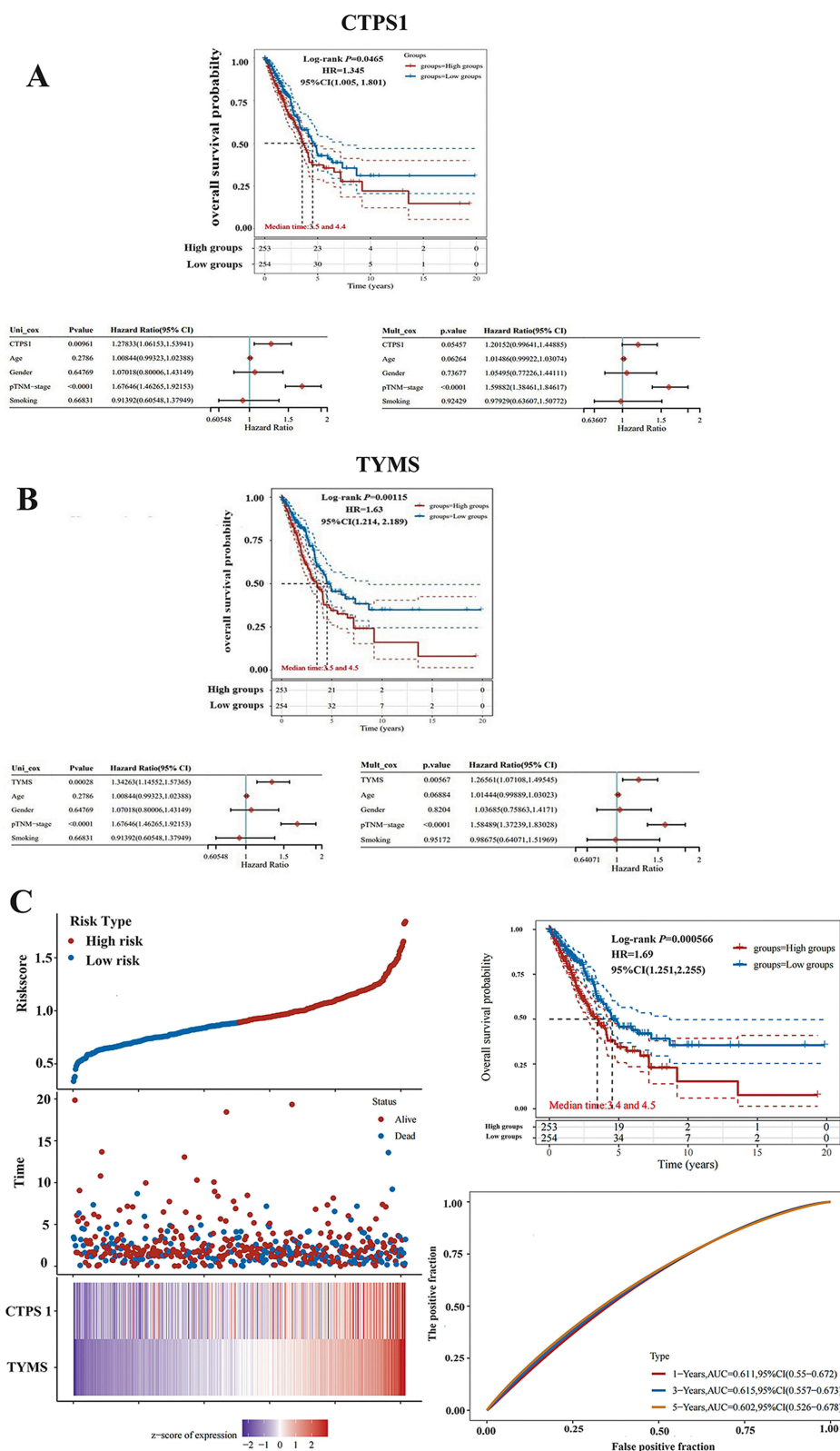


Figure 6 Differential expression proteins of nucleotide metabolism for predicting survival outcomes. The Kaplan-Meier survival analysis and COX regression analysis were conducted on the CTPS1 (**A**) and TYMS (**B**) using data from the TCGA dataset. (**C**) The distribution of risk scores, survival analysis, and heatmap visualization for patients with a double-gene signature. Upper left: The scatter plot represented the risk score from low to high. Different colors represented different groups. Upper right: Kaplan-Meier survival analysis of the risk model from dataset, comparison among different groups was made by Log rank test. Lower left: the scatter plot distribution represented the risk score of different samples corresponding to the survival time and survival status. The bottom heatmap was the gene expression from the signature. Lower right: the ROC curve of the genes.

Data Sharing Statement

All data generated and/or analyzed during the present study are included in the published article.

Ethics Approval

The study was approved by the Ethical Committee of Jinan Central Hospital, Shandong First Medical University. This study followed the Helsinki declaration (guidelines Helsinki).

Funding

This work was supported by Youth Project of Natural Science Foundation of Shandong Province (ZR2022QH187); Shandong Province Traditional Chinese Medicine Science and Technology Project (Q-2022004).

Disclosure

The authors report no conflicts of interest in this work.

References

- Bray F, Laversanne M, Sung H, et al. Global cancer statistics 2022: GLOBOCAN estimates of incidence and mortality worldwide for 36 cancers in 185 countries. *CA Cancer J Clin*. 2024;74(3):229–263. doi:10.3322/caac.21834
- Bach PB, Cramer LD, Warren JL, Begg CB. Racial differences in the treatment of early-stage lung cancer. *N Engl J Med*. 1999;341(16):1198–1205. doi:10.1056/NEJM199910143411606
- National comprehensive cancer network (NCCN) non-small cell lung cancer guidelines version 3.2024. Available from: <https://www.nccn.org/guidelines/guidelines-detail?category=1&id=1450>. Accessed March 31, 2025.
- Ni Y, Huang G, Yang X, et al. Microwave ablation treatment for medically inoperable stage I non-small cell lung cancers: long-term results. *Eur Radiol*. 2022;32(8):5616–5622. doi:10.1007/s00330-022-08615-8
- Lu Q, Cao W, Huang L, et al. CT-guided percutaneous microwave ablation of pulmonary malignancies: results in 69 cases. *World J Surg Oncol*. 2012;10:80.
- Vogl TJ, Worst TS, Naguib NN, Ackermann H, Gruber-Rouh T, Nour-Eldin NE. Factors influencing local tumor control in patients with neoplastic pulmonary nodules treated with microwave ablation: a risk-factor analysis. *AJR Am J Roentgenol*. 2013;200(3):665–672. doi:10.2214/AJR.12.8721
- Zheng A, Ye X, Yang X, Huang G, Gai Y. local efficacy and survival after microwave ablation of lung tumors: a retrospective study in 183 patients. *J Vasc Interv Radiol*. 2016;27(12):1806–1814. doi:10.1016/j.jvir.2016.08.013
- Vogl TJ, Eckert R, Naguib NN, Beeres M, Gruber-Rouh T, Nour-Eldin NA. Thermal ablation of colorectal lung metastases: retrospective comparison among laser-induced thermotherapy, radiofrequency ablation, and microwave ablation. *AJR Am J Roentgenol*. 2016;207(6):1340–1349. doi:10.2214/AJR.15.14401
- Vogl TJ, Naguib NN, Gruber-Rouh T, Koitka K, Lehnert T, Nour-Eldin NE. Microwave ablation therapy: clinical utility in treatment of pulmonary metastases. *Radiology*. 2011;261(2):643–651.
- Peng B, Ling X, Huang T, Wan J. HSP70 via HIF-1 α SUMOylation inhibits ferroptosis inducing lung cancer recurrence after insufficient radiofrequency ablation. *PLoS One*. 2023;18(11):e0294263.
- Wan J, Wu W, Chen Y, Kang N, Zhang R. Insufficient radiofrequency ablation promotes the growth of non-small cell lung cancer cells through PI3K/Akt/HIF-1 α signals. *Acta Biochim Biophys Sin (Shanghai)*. 2016;48(4):371–377. doi:10.1093/abbs/gmw005
- Yan P, Lyu X, Wang S, et al. Insufficient ablation promotes the metastasis of residual non-small cell lung cancer (NSCLC) cells via upregulating carboxypeptidase A4. *Int J Hyperthermia*. 2021;38(1):1037–1051. doi:10.1080/02656736.2021.1947530
- Su X, Wang J, Jiang L, et al. PCNA inhibition enhances the cytotoxicity of β -lapachone in NQO1-positive cancer cells by augmentation of oxidative stress-induced DNA damage. *Cancer Lett*. 2021;519:304–314.
- Lin Y, Zhang J, Li Y, et al. CTPS1 promotes malignant progression of triple-negative breast cancer with transcriptional activation by YBX1. *J Transl Med*. 2022;20(1):17. doi:10.1186/s12967-021-03206-5
- Wu F, Mao Y, Ma T, et al. CTPS1 inhibition suppresses proliferation and migration in colorectal cancer cells. *Cell Cycle*. 2022;21(24):2563–2574. doi:10.1080/15384101.2022.2105084
- Minet N, Bosch AC, Lane R, et al. Differential roles of CTP synthetases CTPS1 and CTPS2 in cell proliferation. *Life Sci Alliance*. 2023;6:. doi:10.26508/lsa.202302066
- Wang L, Shi C, Yu J, Xu Y. FOXM1-induced TYMS upregulation promotes the progression of hepatocellular carcinoma. *Cancer Cell Int*. 2022;22(1):47.
- Karimi L, Jaber M, Asadi M, et al. Significance of microRNA-330-5p/TYMS expression axis in the pathogenesis of colorectal tumorigenesis. *J Gastrointest Cancer*. 2022;53(4):965–970. doi:10.1007/s12029-021-00695-x
- Zhao M, Tan B, Dai X, et al. DHFR/TYMS are positive regulators of glioma cell growth and modulate chemo-sensitivity to temozolomide. *Eur J Pharmacol*. 2019;863:172665. doi:10.1016/j.ejphar.2019.172665
- Mullen NJ, Singh PK. Nucleotide metabolism: a pan-cancer metabolic dependency. *Nat Rev Cancer*. 2023;23(5):275–294.
- Peters GJ, Backus HH, Freemantle S, et al. Induction of thymidylate synthase as a 5-fluorouracil resistance mechanism. *Biochim Biophys Acta*. 2002;1587(2–3):194–205. doi:10.1016/s0925-4439(02)00082-0
- Shih C, Chen VJ, Gossett LS, et al. LY231514, a pyrrolo [2,3-d] pyrimidine-based antifolate that inhibits multiple folate-requiring enzymes. *Cancer Res*. 1997;57(6):1116–1123.

23. Cerqueira NM, Fernandes PA, Ramos MJ. Understanding ribonucleotide reductase inactivation by gemcitabine. *Chemistry*. 2007;13(30):8507–8515. doi:10.1002/chem.200700260
24. Yuan Z, Wang Y, Zhang J, Zheng J, Li W. A meta-analysis of clinical outcomes after radiofrequency ablation and microwave ablation for lung cancer and pulmonary metastases. *J Am Coll Radiol*. 2019;16(3):302–314. doi:10.1016/j.jacr.2018.10.012
25. Moussa AM, Ziv E, Solomon SB, Camacho JC. Microwave ablation in primary lung malignancies. *Semin Intervent Radiol*. 2019;36(4):326–333. doi:10.1055/s-0039-1700567

OncoTargets and Therapy

Publish your work in this journal

OncoTargets and Therapy is an international, peer-reviewed, open access journal focusing on the pathological basis of all cancers, potential targets for therapy and treatment protocols employed to improve the management of cancer patients. The journal also focuses on the impact of management programs and new therapeutic agents and protocols on patient perspectives such as quality of life, adherence and satisfaction. The manuscript management system is completely online and includes a very quick and fair peer-review system, which is all easy to use. Visit <http://www.dovepress.com/testimonials.php> to read real quotes from published authors.

Submit your manuscript here: <https://www.dovepress.com/oncotargets-and-therapy-journal>

Dovepress
Taylor & Francis Group